Short-pulse properties of optical frequency comb generators

Richard P. Kovacich, Uwe Sterr, and Harold R. Telle

An optical frequency comb generator, based on a simple electro-optic modulator in an optical resonator, can produce high-repetition-rate picosecond pulses. Unlike conventional picosecond lasers, the properties of these pulses are greatly affected by detuning the optical cavity and by dispersion caused by the electro-optic crystal. Picosecond pulses were studied in a physical device by numerical simulation and intensity autocorrelation measurements. The pulse width and pulse-to-pulse spacing were greatly affected by detuning the input laser frequency and the resonance of the optical resonator, and the numerical simulations showed that dispersion causes temporal ripples that are antisymmetric between pulse pairs.

OCIS codes: 120.3930, 230.2090, 230.4110, 260.2030, 320.5550.

1. Introduction

Short-pulse lasers are increasingly being used in many areas of science and engineering. Recently experiments show that short-pulse lasers can be used for optical frequency synthesis applications such as frequency metrology, laser spectroscopy, and optical communication.[1] It has been demonstrated that optical frequency comb generators (OFCG's), based on a simple electro-optic modulator inside an optical resonator, can produce picosecond optical pulses,[2] however, pulses as short as a few hundred femtoseconds also seem possible.

Most work with OFCG's has been concentrated on their ability to produce a broad spectrum of equally spaced optical frequencies, i.e., an optical frequency comb. In this respect, OFCG's have been superseded by recent developments in which passively mode-locked femtosecond lasers were used.[3] The use of OFCG's is still popular because they are simple compact devices that can produce short optical pulses with extremely high repetition rates (up to 30 GHz) for any wavelength over the visible to infrared spectrum, making them attractive for integrated-optic applications, especially since the fabrication techniques are good for electro-optic materials such as $LiNbO_3$. Although miniaturization has recently been achieved with monolithic mode-locked semiconductor lasers,[4] they can operate only at fixed wavelengths, whereas an OFCG can easily be used at any wavelength because the optical signal is external. OFCG's are low-power devices, typically having an output of a few milliwatts, but the use of readily available semiconductor power amplifiers allows much higher output if required.[5]

To produce short optical pulses with OFCG's there must be a phase coupling of the cavity modes. In an OFCG this is actively provided by an electro-optic modulator (EOM) inside an optical resonator, in the same way as for much an active frequency-modulated mode-locked laser. The sidebands generated by phase modulation are resonant with the resonator modes by driving the EOM with a frequency equal to an integer multiple of the free spectral range of the optical resonator. The optical signal effectively makes multiple passes through the EOM and, after each pass, extra modulation sidebands are acquired, thus producing a wide-span optical frequency comb that is phase coherent. The sideband power decreases exponentially with sideband order and is well approximated by Eq. (1),[6] where P_k is the power in the kth sideband, β is the single-pass modulation

R. P. Kovacich (rkovacic@ieee.org) is with the Department of Physics, University of Western Australia, Nedlands 6907, W.A. Australia. U. Sterr and H. R. Telle are with the Physikalisch-Technische Bundesanstalt, Bundesallee 100, D-38116 Braunschweig, Germany.

Received 14 March 2000; revised manuscript received 14 March 2000.

0003-6935/00/244372-05$15.00/0

through the EOM, and F is the finesse of the optical resonator:

$$P_k = P_0 \exp\left(\frac{-\pi|k|}{\beta F}\right). \quad (1)$$

However, the production of sidebands that are resonant with resonator modes cannot continue indefinitely because of dispersion in the EOM, which shifts the cavity resonances off the modulation sidebands. This dispersion limit produces a sharp cutoff at the optical frequency comb spectrum, limiting its span to[7]

$$\Delta f = \frac{[2(-\beta' + \beta)M]^{1/2}}{\pi}, \quad (2)$$

where M is related to the EOM material dispersion by $M = (2\pi c/D\lambda_0{}^2 L_c)$, where D is the material dispersion defined as

$$D = \frac{\lambda_0}{c}\frac{\partial^2 n}{\partial \lambda^2}{}_{\lambda=\lambda_0},$$

λ_0 is the input laser wavelength in vacuum, L_c is the EOM crystal length, and c is the speed of light in vacuum. This can be related to the group velocity dispersion (GVD) by use of GVD $\cong (D\lambda_0{}^2/2\pi c)$. β' is the normalized detuning between the input laser frequency ν_0 and the nearest cavity resonance ν_R, defined as $\beta' = [\pi(\nu_0 - \nu_R)]/\mathrm{FSR}$ where FSR is the free spectral range of the optical resonator.

The output of the OFCG can be understood in the time domain as follows. Because of phase modulation, the resonator has an instantaneous resonance frequency $\nu_{\mathrm{res}}(t)$ defined by

$$2\pi L_{\mathrm{opt}}\nu_{\mathrm{res}}(t)/c + 2\phi_m(t) = 0 \bmod 2\pi, \quad (3)$$

where L_{opt} denotes the optical round-trip length of the resonator, $\phi_m = \beta \sin(2\pi\nu_m t)$, the instantaneous single-pass phase shift that is due to the EOM, and t is the delayed time. Because of the periodic modulation, field components injected at a frequency ν_0 that fulfill Eq. (3) at a certain time superimpose at each round trip at a fixed modulation angle ϕ_m and add up constructively, leading to a periodic gating characteristic. In particular, if the injected input frequency is near the instantaneous frequency during the linear sweep of the sampling function ($\beta' = 0$), this leads to a Lorentzian sampling function and thus to two Lorentzian output pulses per modulation period. Neglecting dispersion and losses, the peak power of the pulses is equal to the input cw power, and the average power P_{av} is given by the effective duty angle of the sampling process, leading to

$$P_{\mathrm{av}} \propto (1 - \beta/\beta')^{-1}. \quad (4)$$

Including dispersion leads to broadened pulses and adds temporal ripples.

Parameter β' is the most critical in practice because it is highly sensitive to fluctuations of the cavity length and input laser frequency. It has a significant influence on the OFCG span, as shown by Eq. (2), and also on the pulse-to-pulse spacing or timing jitter. Hence, techniques have been developed to stabilize β'.[7,8] When $\beta' = 0$, the pulses are evenly spaced inasmuch as the pulses occur when the microwave field across the EOM is zero, i.e., twice per microwave cycle (assuming a modulation amplitude of $\beta' < \pi/2$). But if β' is nonzero, the pulse-to-pulse spacing becomes uneven, and hence any fluctuations will produce timing jitter. The pulse width is also at its minimum when $\beta' = 0$ because the sampling function has the steepest slope. As the pulse width is mostly affected by the low-order sidebands that contain most of the power, this setting does not lead to the widest spectrum as given in Eq. (1). The broadest spectrum is obtained for $\beta' = -\beta$, when the dispersion is balanced with a properly detuned β'.

Although pulses from OFCG's have been considered for $\beta' = 0$,[2,9] the quantitative effect of dispersion and a detuned β' on the pulse characteristics has not been studied previously. Here we investigate these pulses by numerical simulations based on the solution of coupled-cavity mode equations for a physical OFCG. The numerical simulations were verified by intensity autocorrelation measurements of the OFCG output.

2. Numerical Modeling

In the following we present a numerical analysis of the OFCG in the Fourier domain, including dispersion and arbitrary experimental parameters. Because of the periodicity of the modulation, in the steady state the optical field inside the OFCG can be expanded in terms of the modulation sidebands of the incident field:

$$E(t) = \sum_k E_k \exp[2\pi j(\nu_0 + k\nu_m)t], \quad (5)$$

where E_k is the complex field amplitude of the kth sideband, ν_0 is the incident optical frequency, and ν_m is the modulation frequency. The complex field amplitudes of each sideband are related by a set of linear equations that describe their mutual coupling. With appropriate boundary conditions, such as the input field, an unambiguous solution can be found.

In a linear cavity, the Fourier components $E_k{}'$ after one round trip with input field $E_k{}^{\mathrm{in}}$ are given by

$$E_k{}' = r_1 r_2 \exp(2j\phi_k) \sum_q J_q(2\beta) E_{k-q} + t_1 E_k{}^{\mathrm{in}}, \quad (6)$$

where r_1 and r_2 are the complex amplitude reflectivities of the input and the output mirrors, respectively, that describe the loss for each mode, and t_1 is the amplitude transmission of the input coupler. The coupling between modes is described by the Bessel function $J_q(2\beta)$ and the round-trip phase shift ϕ_k of mode k. The round-trip phase shift is given by[7]

$$\phi_k = \beta' + k\frac{\pi\Delta\nu_m}{\mathrm{FSR}} + \frac{k^2}{2}\mathrm{GVD}\, L_c(2\pi\nu_m)^2 \quad (7)$$

The first term is due to detuning the carrier from the cavity resonance, the linear term in the sideband order describes the detuning of the modulation frequency from the FSR of the cavity denoted by $\Delta\nu_m$, and the last term is due to dispersion in the EOM crystal.

Writing the Fourier amplitudes as vector $\mathbf{E}$, the requirement for self-consistency of Eq. (7), $\mathbf{E}' = \mathbf{E}$, leads to a coupled-mode equation:

$$\mathbf{E} = \mathcal{M}\boldsymbol{E} + \mathbf{E}_{\text{in}}. \tag{8}$$

The square matrix $\mathcal{M}$ contains the coefficients from Eq. (6) for a sufficiently large number of sidebands that are required to describe the total electric field. The coupling between the sidebands with a different order number q caused by phase modulation is proportional to the Bessel functions $J_q(2\beta)$. Because this coupling decreases rapidly with order q, it is sufficient here to consider only $|q| < 15$. Therefore $\mathcal{M}$ becomes a banded matrix of bandwidth $2q + 1$, and the problem was effectively reduced to a solution of the 1024×1024 sparse matrix equation. The complex field amplitudes completely describe the magnitude and the phase of the OFCG output spectrum. A Fourier transformation allows the time structure, and, hence, the intensity autocorrelation function, to be determined.

3. Experiments

The OFCG consisted of a 1 mm $\times$ 1 mm $\times$ 25 mm $LiNbO_3$ EOM crystal in the middle of a Fabry–Perot cavity. To achieve maximum modulation we mounted the crystal inside a rectangular microwave cavity resonant with a microwave signal, in such a way that the group velocity of the microwave signal was equal to the optical phase velocity.[10] The Fabry–Perot cavity was formed by two curved mirrors with -100-mm radius of curvature, separated by approximately 130 mm. One of the mirrors was mounted on a piezoelectric transducer, which allowed us to adjust β' by changing the resonance frequencies of the Fabry–Perot cavity. The optical signal at 850 nm was provided by a 100-mW laser diode, injection locked to an extended cavity laser diode. To prevent feedback into the laser diodes we used optical isolators. A finesse of $F = 50$ was achieved in the Fabry–Perot cavity. The fundamental TE mode of the microwave cavity was at $\nu_m = 8.73$ GHz, and the mirror separation was manually adjusted so the resonance condition was met, which corresponded to $\nu_m = 7$ FSR. As much as 12 W of power could be coupled into the microwave cavity, but, to avoid excessive heating and the need for temperature control, we used only 5 W. This allowed us to obtain $\beta = 0.9$. The OFCG was operated without a stabilization system, because β' was already stable enough to be used for the measurements.

We measured the intensity autocorrelation function by using the autocorrelator shown in Fig. 1. Because of the low output power from the OFCG (1-mW peak intensity), a sensitive detection system and a highly efficient autocorrelator crystal were required. A 5-mm-long lithium iodate ($LiIO_3$) crystal was used to generate the sum-frequency autocorrelation signal, and this was angle phase matched to the input beams that were crossed to maximize the contrast. The input beams were also focused to optimize the nonlinear efficiency of the crystal, but, because of the large walk off in $LiIO_3$, the focusing could only be moderate. The autocorrelation signal was measured by a photomultiplier connected to a lock-in amplifier detection system, and the high sensitivity was essential because signals as low as 10 fW had to be measured. An adjustable time delay was provided in one arm by a retroreflector on a translation stage. The resolution of this autocorrelator is limited by dispersion in the crystal, and, for a 5-mm-long crystal, the resolution is approximately 100 fs, far below the experimental pulse length. We measured the detuning parameter β' by monitoring the output power of the OFCG as a function of β' and by noting its position relative to the power minimum that coincided with $\beta' = 0$ as given by relation (4).

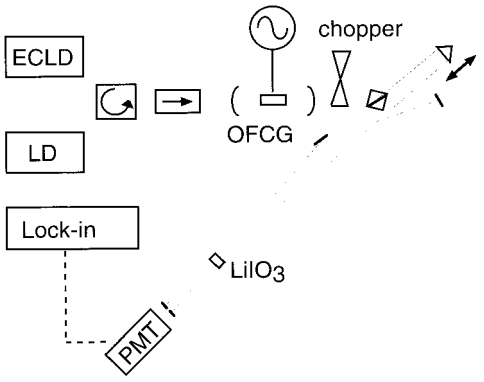

Fig. 1. Diagram of the autocorrelator that we used for the OFCG experiment: ECLD, extended cavity laser diode; LD, laser diode; PMT, photomultiplier tube.

According to Eq. (1), the OFCG spectrum should decrease at a rate of 35 dB/THz for $\beta = 0.9$ and $F = 50$ when $\beta' = 0$. We measured this by heterodyning the output of the OFCG with an additional tunable extended cavity laser diode. The beat signal between the laser and the nearest OFCG sideband was detected by a fast photodetector (100-MHz bandwidth) and displayed on a spectrum analyzer. The measured sideband signals are shown in Fig. 2, and they agree with the modeled curve. This was also done for $\beta' = \beta$ and $\beta' = -\beta$. The spectrum decreases more rapidly as expected, however there is only a slight difference between the two detuning cases where the vast majority of power is concentrated, i.e., for modulation sidebands close to the optical carrier. The difference can be seen only in the low-energy wings of the spectrum, which is shown in Fig. 3. This also applies to other values of β', and therefore the pulse shapes for positive and negative β' are essentially the same.

The measured intensity autocorrelation functions for $\beta' = 0$ and $\beta' = -0.9$ are shown in Fig. 4, and

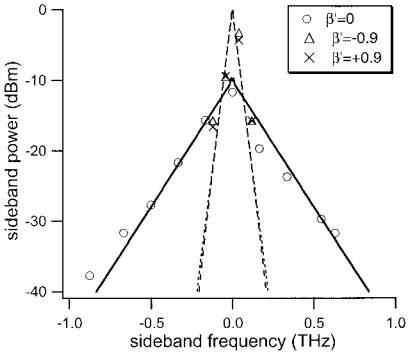

Fig. 2. Measured OFCG sidebands, showing that the OFCG spectrum becomes narrower as β' is detuned. The solid curves show the modeled spectrum.

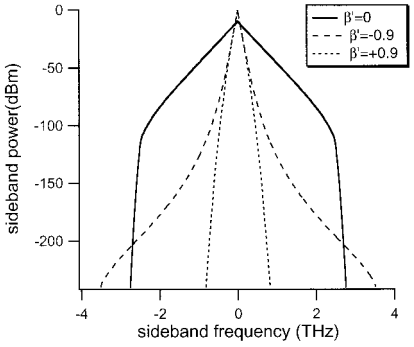

Fig. 3. Modeled OFCG spectra showing the dependence on β' detuning and the sharp cutoff that is due to dispersion limits. The difference between $\beta' > 0$ and $\beta' < 0$ can be seen only at the low-energy wings of the spectra.

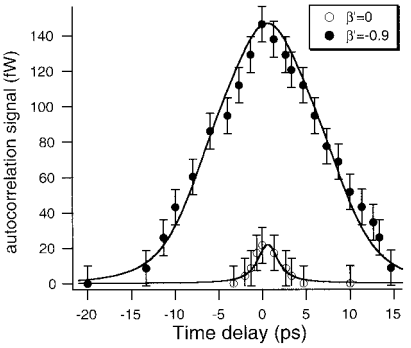

Fig. 4. Measured intensity autocorrelation functions, showing that the pulse width and intensity increase as β' is detuned. The solid curves show the modeled intensity autocorrelation functions.

again the solid curves show the numerical model that is in agreement. Figure 4 demonstrates that the pulse width and the intensity increase as β' is detuned inasmuch as the OFCG spectrum becomes narrower. Assuming a Lorentzian pulse shape, the minimum pulse width was 1.6 ps FWHM, i.e., half of the autocorrelation width.[11] According to Kobayashi *et al.*,[9] the pulse width is approximately given by

$$\tau_p = \frac{1}{2\beta F \nu_m}. \tag{9}$$

For the OFCG that was used in this experiment, we expect $\tau_p = 1.3$ ps. The presence of dispersive effects leads to a slightly higher result.

4. Discussion

The consistent agreement between the measured results and the modeled curves gave validity to the numerical modeling, and therefore the time structure of the pulses could be deduced from the numerical model. The time structure of the OFCG pulses for various β' is shown in Fig. 5. As explained in Section 1, the pulses occur when the Fabry–Perot cavity is resonant with the input laser frequency. When $\beta' = 0$, the cavity is in resonance when the corresponding electric field across the EOM crystal is zero. In this situation two evenly spaced pulses occur during the sinusoidal modulation period. If β' is detuned, however, the cavity comes into resonance when the electric field across the EOM crystal is nonzero. Therefore pulse spacing becomes uneven because the pulses occur close together on one half of the modulation period, and, as $\beta' = \beta$ is approached, the two pulses merge to form a single broad pulse that occurs once per modulation period.

Time t at which the pulses occur, follows from Eq. (3) and is approximately given by the solution to

$$0 = \beta' - \beta \sin(2\pi\nu_m t) - N\pi. \tag{10}$$

If $\beta < \pi/2$ (as was the case in this experiment), then solutions exist only for $N = 0$, i.e., only one cavity resonance is used. But for $\beta > \pi/2$, solutions also exist for $N = 1$, because the electric field across the EOM crystal is sufficient to move the resonant fre-

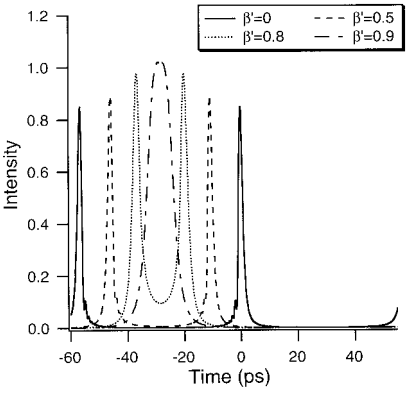

Fig. 5. Modeled time structure of the OFCG pulses, showing that pulse spacing becomes uneven as β' is detuned.

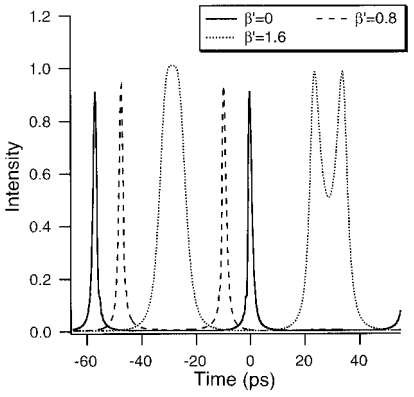

Fig. 6. Modeled time structure for the OFCG pulses if $\beta > \pi/2$. A new pair of pulses begins to form on the other half of the modulation cycle as β' approaches $\pi/2$.

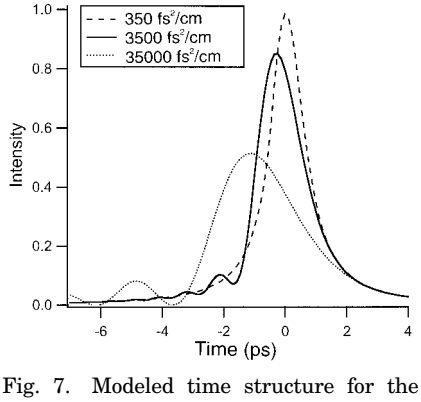

Fig. 7. Modeled time structure for the OFCG pulses assuming different GVD in EOM crystal. The phase shift caused by the dispersion produces temporal ripples and broadens the pulses.

quency of the cavity by one FSR. Figure 6 illustrates this situation. As β approaches $\pi/2$, another pair of pulses begins to form during the other half of the modulation period.

The timing jitter δt that is due to frequency fluctuations $\delta\nu_0$ of the input laser frequency can be crudely estimated from a Taylor series expansion of Eq. (10) in a quasi-static approximation, i.e., for frequency fluctuations slower than the storage time of the optical resonator. Using $\delta\beta' \cong (\pi/\mathrm{FSR})\delta\nu_0$, the perturbation term gives the following estimate for the timing jitter:

$$\delta t = \frac{\delta\nu_0}{2\beta\nu_m \mathrm{FSR}\cos(2\pi\nu_m t)}. \tag{11}$$

It becomes more sensitive as β' approaches β because $\cos(2\pi\nu_m t) \to 0$. Equation (11) blows up if $\beta' = \beta$, where the approximation is no longer valid. For an extended cavity laser diode $\delta\nu_0 \approx 1$ MHz, and this leads to a timing jitter of approximately 0.05 ps at $\beta' = 0$.

The GVD in the EOM crystal also influences the pulse shape, as shown in Fig. 7 for hypothetically different GVD values from the actual GVD of $LiNbO_3$, which is 3500 fs^2. GVD broadens the pulse and adds temporal ripples, which skews the pulse toward the trailing edge if the electric field across the EOM crystal is on the increase. In Eq. (6) the dispersion adds a quadratic phase shift between adjacent sidebands k and $k + 1$ of the form $\exp[jb\,(i\nu_m)^2]$, where $b \cong \mathrm{GVD}L_c(2\pi)^2$. This leads to a cubic phase shift and to a convolution in the time domain that produces the temporal ripples. A phase reversal occurs between consecutive pulses, so the ripples are antisymmetric between pulse pairs, which can be seen in Fig. 5. The dispersion also produces a sharp cutoff at the OFCG spectrum, which is evident in Fig. 3, but the spectral windowing caused by this is not responsible for any significant structure on the pulses as the power near the dispersion limit is negligible. Although the period of ripples is not constant, it approximately equals $\sqrt{4b}$, and this depends only on the GVD and the length of the EOM crystal. The ripple period also provides an estimate of the minimum pulse width attainable, which for the OFCG that we used in this experiment, is approximately 1 ps. To obtain a shorter pulse width the EOM crystal must be shortened to reduce dispersion, but this would also reduce the modulation index.[6] A more elaborate solution would be to use dispersion-compensating elements in the cavity,[12] but this would complicate the design of the OFCG.

5. Conclusion

The short-pulse properties of an OFCG have been investigated by numerical simulations that were verified by measurements of the output spectrum and the intensity autocorrelation function. It has been shown that pulse spacing becomes uneven as β' is detuned, and as β' approaches β the pulse pairs merge to form a single broad pulse. Therefore changes in β' caused by fluctuations of the input laser frequency lead to timing jitter of the OFCG pulses. In addition to the timing, the structure of the individual pulses also depends on β' and dispersion in the EOM crystal; the pulse width increases as β' is detuned, and the dispersion creates temporal ripples that are antisymmetric between pulse pairs. These OFCG pulses offer great flexibility and control of picosecond optical pulses in a simple compact system that can be used at any wavelength for which transparent electro-optic crystals are available.

References

1. T. Udem, J. Reichert, R. Holzwarth, and T. W. Hänsch, "Accurate measurement of large optical frequency differences with a mode-locked laser," Opt. Lett. **24,** 881–883 (1999).
2. G. M. Macfarlane, A. S. Bell, E. Riis, and A. I. Ferguson, "Optical comb generator as an efficient short-pulse source," Opt. Lett. **21,** 534–536 (1996).
3. H. R. Telle, G. Steinmeyer, A. E. Dunlop, J. Stenger, D. H. Sutter, and U. Keller, "Carrier-envelope offset phase control: a novel concept for absolute optical frequency measurement and ultrashort pulse generation," Appl. Phys. B **69,** 327–332 (1999).
4. S. Arahira, Y. Matsui, T. Kunii, S. Oshiba, and Y. Ogawa, "Transform-limited optical short-pulse generation at high repetition rate over 40 GHz from a monolithic passive mode-locked DBR laser diode," IEEE Photon. Technol. Lett. **5,** 1362–1365 (1993).
5. K. Imai, M. Kourogi, and M. Ohtsu, "30-THz span optical frequency comb generation by self-phase modulation in an optical fiber," IEEE J. Quantum Electron. **34,** 54–60 (1998).
6. M. Kourogi, K. Nakagawa, and M. Ohtsu, "Wide-span optical frequency comb generator for accurate optical frequency difference measurement," IEEE J. Quantum Electron. **29,** 2693–2701 (1993).
7. M. Kourogi, B. Widiyatomoko, Y. Takeuchi, and M. Ohtsu, "Limit of optical-frequency comb generation due to material dispersion," IEEE J. Quantum Electron. **31,** 2120–2125 (1995).
8. U. Sterr, B. Lipphardt, A. Wolf, and H. R. Telle, "A novel stabilization method for an optical frequency comb generator," IEEE Trans. Instrum. Meas. **48,** 574–577 (1999).
9. T. Kobayashi, T. Sueta, Y. Cho, and Y. Matsuo, "High-repetition rate optical pulse generator using a Fabry–Perot electro-optic modulator," Appl. Phys. Lett. **21,** 341–343 (1972).
10. M. Kourogi, "Optical frequency comb generators and their applications," in *Frequency Control of Semiconductor Lasers*, M. Ohtsu, ed. (Wiley, New York, 1996), pp. 95–135.
11. K. L. Sala, A. K. Wallace, and G. E. Hall, "CW autocorrelation measurements of picosecond laser pulses," IEEE J. Quantum Electron. **QE-16,** 990–996 (1980).
12. L. R. Brothers and N. C. Wong, "Dispersion compensation for terahertz optical frequency comb generation," Opt. Lett. **22,** 1015–1017 (1997).